激光与光电子学进展

Spin of Micro-Propeller Structures Driven by High-Order Poincaré Beams

Lin Qian, Chen Lei, Zhuang Zikuan, Sun Jingxuan, Zhang Li*, Xie Jianing**

Guangdong-Hong Kong-Macao Joint Laboratory for Intelligent Micro-Nano Optoelectronic Technology, Foshan University, Foshan 528225, *Guangdong, China*

Abstract The use of light-induced micro-motors or micro-propellers, showcasing non-contact and non-damaging characteristics, is garnering increased attention in biomedical, micro-machine, and environmental fields. The High-order Poincaré (HOP) beam, as a vector beam, provides a controllable driving force with adjustable orbital angular momentum and spin angular momentum. In this study, we present the spin of a self-assembled micro-propeller structure propelled by the HOP beam, enabling flexible control over rotation velocity and direction. Our findings reveal that modifications to the total angular momentum of the driving beam field or alterations in the micro-propeller blade structure can influence rotation velocity. This research offers an efficient and versatile approach for applications in optical micromanipulation and micromachinery.

Key words high-order Poincaré beam; self-assemble propeller; micro-propeller

中图分类号 TN247 **文献标志码** A **DOI**: 10.3788/LOP232362

1 Introduction

Since Ashkin et al. [1] firstly demonstrated optical manipulation on micro or nano-size particles by a single beam, optical tweezers have quickly become a significant tool to manipulate small objects in biomedicine[2-4] and physics[5-7] fields due to its advantages of non-contact and non-damage[8-10]. With the development of structured light, the manipulation methods of optical tweezers have been gradually diversified. In particular, the vector beam, whose polarization varies with space, can perform more novel and interesting capture phenomenon. For example, radial polarization vector beam can realize highly efficient three-dimensional capture of nano-metal particles[11]. Meanwhile, the tightly focused radial polarization vector beam can selectively capture chiral nanoparticles[12]; Azimuth polarization vector beam has advantages in transverse trapping of nanoscale metal particles[13], while tightly focused azimuth polarization vector beam can capture multiple particles simultaneously[14].

Vector beams carries spin angular momentum (SAM) determined by polarization and orbital angular momentum (OAM) determined by topological charge[15], which can drive particles to rotate. Rotation motion induced by SAM and OAM has been utilized in many fields, including opto-mechanics, cold atom, and biology fields[16-18]. Specially, such rotation phenomenon accelerates the development of micromotors or micro-propellers, which brings many opportunities in drug delivery, micro-surgery, sensing[19-21], and so on. Due to its ability to remotely control propagation and further control the motion of motors or propellers by regulation of SAM and OAM, light has been proven to be an effective driving force. Thus, the movement of micromotors and micro-propellers exploiting vector beams has become the latest research trends. For instance, Laguerre-Gauss (LG) beams with OAM and SAM can induce rotation of propeller which consists of single silver (Ag) nanowires, silicon nanorods and gold nanorod respectively[22-24]. Recently, four motors composed microdrones can be driven by a light, which performs translational and rotational motion in an aqueous environment[25].

In general, the driving force about rotation of micromotors or micro-propellers comes from the SAM and OAM of light. Changing the polarization state can control the SAM, which allows the spin velocity of the

收稿日期: 2023-09-24; **修回日期**: 2023-10-24; **录用日期**: 2023-11-17; **网络首发日期**: 2023-12-12

基金项目: 国家自然科学基金 (62105062)

通信作者: *zhangli4102@126.com; **xiejianingfs@126.com

particle adjustable. However, the value of SAM can only be ±1, thereby imposing constrains on the velocity. By contrast, OAM is more flexible and can be extended to any integer or even fractional order, but the beam diameter is affected by the OAM. A larger OAM will yield a larger beam diameter, which may bring new challenges to the optical manipulation. Actually, the rotational motion can be divided into "spin" and "orbit" based on the rotating axis, but they are not necessarily confined to corresponding angular momentum of light. Here, we report a self-assembling propeller that is driven by a high order Poincaré (HOP) beam. We utilize the beam to assemble the micro-propeller under zero total angular momentum conditions, and to drive the micro-propeller to spin under non-zero total angular momentum conditions. By adjusting the blades of propeller and the total OAM of beam, the propeller rotating velocity can be controlled. Furthermore, since the total OAM of HOP beam depends on the optical field profile parameters instead of the topological charge, the diameter of beam keep constant, which yield the stable rotation of micro-propeller. Our work provides a flexible approach in micromanipulation and micromachinery.

2 Method

Theoretically, an arbitrary HOP beam is formed by superposition of two orthogonal conjugate circularly polarized LG beams whose orders are negative to each other [26-27].

$$\boldsymbol{E}(r,\varphi)=A\cdot LG_0^{l}(r,\varphi)\hat{e}_r+B\cdot LG_0^{-l}(r,\varphi)\hat{e}_l\ , \tag{1}$$

where $\hat{e}_r$ and $\hat{e}_l$ are two unit-vectors of the right-handed and left-handed circular components, respectively. A and B are two controllable optical field profile parameters, which are used to adjust the profile of the HOP beam. $LG_0^{l}(r,\varphi)$ and $LG_0^{-l}(r,\varphi)$ represent beams carrying orbital angular momentum of l and $-l$, respectively. Here l is an integer, representing the topological charge of the vortex. LG beam of $p=0$ can be described as

$$LG_0^{l}(r,\varphi)=E_0 r^{|l|}L_0^{|l|}\left(\frac{2r}{w^2}\right)\exp\left(-\frac{r^2}{w^2}\right)\exp(\mathrm{i}l\varphi), \tag{2}$$

where φ is the azimuthal angle, w is the beam waist, and $L_0^{|l|}(\cdot)$ is the relevant Laguerre polynomial. The HOP beam can be generated by the scheme shown in Fig. 1(a). The fundamental Gaussian mode of horizontal polarization is derived from a 1064 nm laser source. Then, after passing half wave plate (HWP) with angle

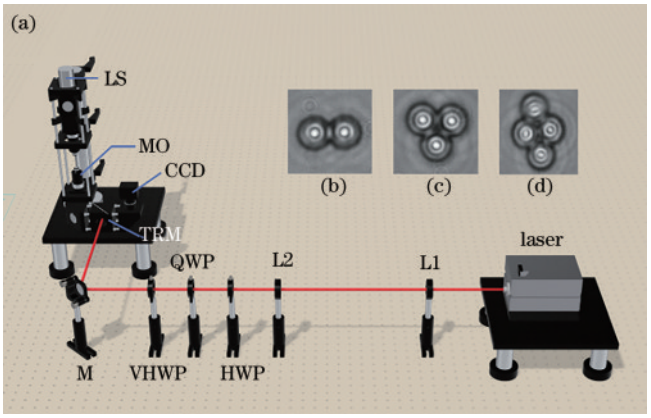

Fig. 1　(a) Experimental setup; (b)-(d) manipulated polystyrene on the loading platform with respect to two-, three- and four-blade structures

α, incident on quarter wave plate (QWP) with angle $-45°$ from the fast axis, the linearly polarized beam is converted to circular polarization. Correspondingly, the beam field can be described as

$$LG_0^{0}(r,\phi)\begin{pmatrix}1\\0\end{pmatrix}\xrightarrow{HWP,QWP}\frac{(1+i)\cos(2\alpha)}{2}LG_0^{0}(r,\phi)\begin{pmatrix}1\\i\end{pmatrix}+\frac{(1-i)\sin(2\alpha)}{2}LG_0^{0}(r,\phi)\begin{pmatrix}1\\-i\end{pmatrix}, \tag{3}$$

where three column Jones matrices represent the horizontal polarization, left- and right-hand circular polarization, respectively (from left to right). Next, the polarization modulated LG beam incident on vortex half wave plate (VHWP) of order l, and the optical field[28] can be described as

$$\frac{(1+i)\cos(2\alpha)}{2}LG_0^{0+l}(r,\phi)\begin{pmatrix}1\\-i\end{pmatrix}+\frac{(1-i)\sin(2\alpha)}{2}LG_0^{0-l}(r,\phi)\begin{pmatrix}1\\i\end{pmatrix}. \tag{4}$$

After passing through the VHWP, the right- and left-hand circular polarization will convert to each other, while the topologic charges are added $+l$ and $-l$, respectively. It can be concluded from Eq. (4) that the parameters of optical field profile of HOP beam are controlled by the included angle between the HWP and the horizontal direction. Therefore, we only need to change the angle of HWP to adjust the value of OAM. Thus, the total OAM of HOP beam can be described as

$$M_{\mathrm{OAM\ total}}\propto(|A|-|B|)\cdot l\ , \tag{5}$$

where $A=\frac{(1+i)\cos(2\alpha)}{2}$ and $B=\frac{(1-i)\sin(2\alpha)}{2}$.

It is shown that the total OAM regulation of HOP beam depends on the optical field profile parameters instead of the topological charge, so the diameter of beam can be fixed in a constant.

In order to avoid not being able to clearly observe the particle rotation and calculate the rotation velocity due to high power, we set the 100× objective (MO, NA=1.25) power at 40 mW. After collimating through the two lenses, the laser beam successively passes through the HWP, the QWP, the VHWP of l=2, and then is focused through the objective lens into the pure water filled with polystyrene particles of diameter about 2.5 μm. The sample was illuminated with a white LED (LS) and recorded with a CCD. Firstly, by adjusting α to obtain A=B, i.e., the total angular momentum is 0, the particles can be assembled into a propeller structure. Although there is no glue to fix each particle, the propeller structure can keep the stable and will not separate or deform during rotating. Here, we assemble two-, three- and four-blade structures, shown as Fig. 1(b)-(d). It is shown that two and four paddle structures have two-fold axes rotational symmetry, while three paddle structure has three-fold axes rotational symmetry. Then, changing α to control the total angular momentum of HOP beam can rotate these microstructural propellers.

3 Result

By adjusting the angle of HWP, we investigate the rotation velocity of the four-blade propeller under different total angular momentums, and the results are shown in Fig. 2(a). When the total momentum is 0, i.e., α=22.5°, the microstructure does not rotate. When the total momentum is 0.1, i.e., α=20.5°, the "propeller" rotates around its symmetry center clockwise. When the total momentum is −0.1, i.e., α=24.5°, the "propeller" rotates counterclockwise. It should be noticed that although the driving force derives from the total angular momentum of HOP beams, the motion of propeller is "spin" rather than "orbital" rotation, because the whole structure rotates around its symmetry center without deformation, as shown in the red rhombus of Fig. 2(a). The motion of two blades on the short diagonal line in rhombus is located on the orbit with smaller radius, while the motion of two blades on the long diagonal line is located on the orbit with larger radius, which is quite different from the orbital motion. Thus, the HOP beam drives the self-assembled structure spin around its symmetry center.

Furthermore, we measure the rotation velocities of two-, three- and four-blades "propeller" under different α values. The rotation process can be recorded as video

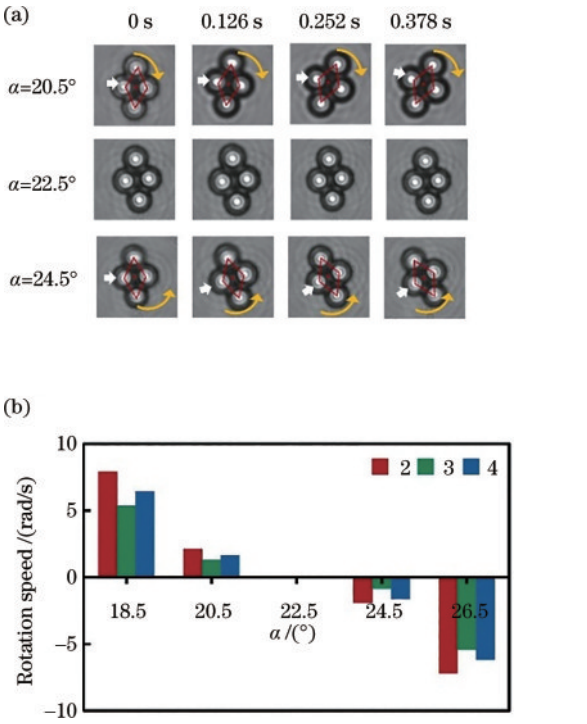

Fig. 2 (a) Rotation of four-blade "propeller" at different α values and time. (the red rhombus denotes the entirety structure of propeller, and the red dot denotes the symmetry center); (b) different combinations of particle steering and α values angle relationship (positive is clockwise, negative is counterclockwise)

and the rotation velocity is calculated by comparing the adjacent frames. Here, we repeated experiment for 4 times under each condition. As shown in Fig. 2(b), the further away from 22.5° is, the faster the "propeller" spin. Besides, two blades rotate faster than four blades, and the three blades rotate slowest. It is clear that the rotation velocity of the "propeller" of this structure is also controlled jointly by the quantity of blades. When α=20.5°, the number of blades perform a little effect on rotate velocity, while the velocity is around 1.65 rad/s. When α=18.5°, the angular velocity of the two-blade "propeller" is 2.68 rad/s faster than that of the three blades, the angular velocity of the four blades is 1.90 rad/s faster than that of the three blades, and the two blades is 0.78 rad/s faster than the four blades. When α>22.5°, the rotation bacome counterclockwise, and the rotation velocity is similar with the case of clockwise. Thus, the overall dynamics of the rotation velocity dependence on the total angular momentum and the micro-structure of objective.

4 Analysis

To further explain that the rotation velocity of

"propeller" is related to the quantity of blades, we conduct simulations of the interaction between different structural "propellers" and HOP beam. In general, the time average optical force acting on a particle can be obtained by considering the integral of Maxwell stress tensor surrounded by a closed surface of a particle:

$$\langle \boldsymbol{F} \rangle = \int_S \boldsymbol{n} \cdot \langle T \rangle \, \mathrm{d}\sigma \,, \tag{6}$$

where, $\boldsymbol{n}$ is the surface normal vector, and T is Maxwell stress tensor.

$$T = \varepsilon \boldsymbol{E}\boldsymbol{E} + \mu \boldsymbol{H}\boldsymbol{H} - \frac{1}{2} I \left(\varepsilon \boldsymbol{E} \cdot \boldsymbol{E}^* + \mu \boldsymbol{H} \cdot \boldsymbol{H}^* \right), \tag{7}$$

where, $\boldsymbol{E}$ and $\boldsymbol{H}$ represent the total electric and magnetic fields outside the particle. For uniform and isotropic particle structures, the electromagnetic field can be solved numerically by using FDTD software.

When the light field interacts with the particle, it is also accompanied by the transfer of angular momentum, resulting in the particle being acted on by torque. For the particle distance from the optical axis $\boldsymbol{x}$, the torque received can be expressed as

$$\langle \boldsymbol{\Gamma} \rangle = \boldsymbol{x} \times \langle \boldsymbol{F} \rangle . \tag{8}$$

Six electromagnetic fields components (E_x, E_y, E_z, H_x, H_y, H_z) of HOP beam on the focal plane are imported into FDTD software. The particles with different microstructures are placed on focal plane, where the symmetry axis coincides with optical axis. Then the optical force and optical torque of the microstructures can be simulated by Eq. (6) and Eq. (8), respectively.

Since the rotation occurs in xy-plane, the force distribution of two, three, four-blade micro-propeller with $\alpha = 12.5^\circ$ at the same power is shown in Fig. 3. The optical force is concentrated in the center of the microsphere, and the direction of the force is always perpendicular to the propeller radius. As a result, the force can drive the propellers rotate. The overall average force per blade is shown in Table 1. The maximum force of two blades is larger than that of three blades and four blades, while the three blades structure performs the smallest force. To illustrate the rotation behavior, the total torque is also calculated shown Table 1. The two-blade structure also performs largest torque, while the three-blade structure performs the smallest torque.

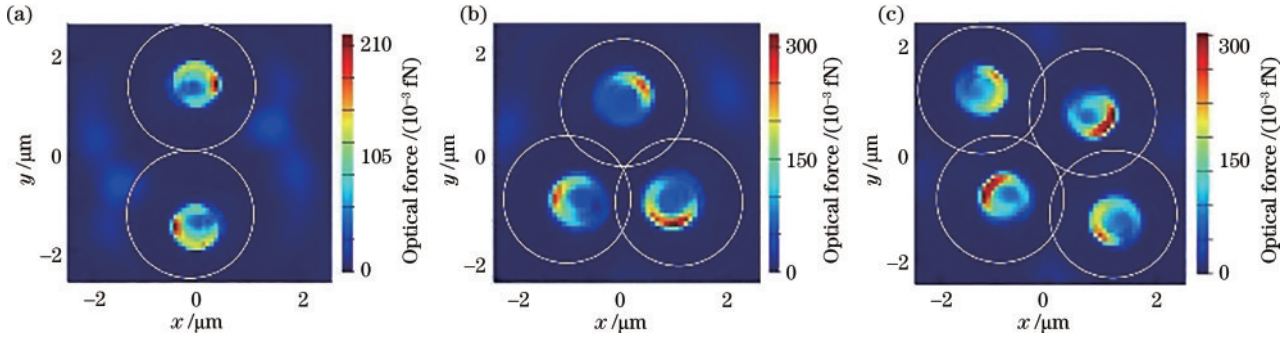

Fig. 3　Force distributions of (a) two-, (b) three- and (c) four-blade per unit volume with the same field when $\alpha = 12.5^\circ$

Table 1　Overall average force and torque of micro-propellers of different structures

Structure	2-blade	3-blade	4-blade
Force /fN	0.2563	0.1914	0.2135
Torque /(fN·μm)	0.3204	0.2354	0.2711

Furthermore, to depict the stable spin rotation of propellers, the resistive forces caused by environment is considered. When the microstructure has size of 0.1—10 μm, its motion in the fluid medium is the application range of low Reynolds number fluid mechanics [29]. In this dimension, fluid inertia can be ignored and the flow field is approximately Stokes fluid. Therefore, the viscous torque[30] expression of a sphere with the same radius is shown as

$$D = 8\pi\mu\omega R^3 \,, \tag{9}$$

where μ is the constant viscosity coefficient, and ω the rotational velocity. Here, we approximate the viscous resistance torque with a spherical structure with the rotational radius R. For the cases of 4 blades, R is taken the average radius between long diagonal and short diagonal into account. Since the propeller is closely connected during rotation, it can be regarded as a whole and the longest rotation axis is taken as the rotation radius. For the steady rotation microstructure, the optical torque and viscous torque should be mechanical equilibrium, and thus the spin velocity can be obtained.

In experiments, the method to measure the rotation velocity follows the previous, so the maximum velocity, minimum velocity and average velocity can be obtained. The velocity of two-, three- and four-blade structures obtained from simulations and experiments

are shown in Fig. 4. It is shown that the simulated results coincide with our experiments. With the angle approaching 22.5°, the total angular momentum decreases to zero and the rotational velocity decreases as well. Meanwhile, at low total angular momentum values ($20.5°<\alpha<22.5°$), the number of blades perform no effect on rotate velocity. When the total angular momentum increases, the number of blades and the total angular momentum play combined role on micro-structure rotation. The interesting phenomena is that the two blades rotate faster than the four blades, and the three blades rotate the slowest under the same angular momentum. A typical example can be referred from the media in supplement, which demonstrate the motion of two-, three- and four-blade structures with $\alpha = 16.5°$. This is because the three-blade structure is relatively stable, and its moment arm is the smallest compared to the other two, so the velocity of the three-blade is the slowest.

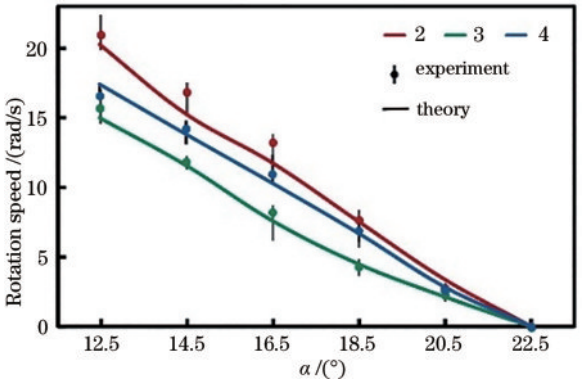

Fig. 4　Theoretical and experimental rotational velocity of propellers self-assembled by two-, three- and four-blade (the line of experimental data denotes the range of velocity, and the dot of experimental data denotes the average velocity)

5　Conclusion

In summary, we demonstrate a light-indued self-assembled propellers to spin by a simple yet flexible method. The HOP beams, whose total angular momentum can be regulated without changing the beam diameter, is introduced to assemble and rotate particles. We found that the velocity control method for the self-assembled "propeller" is not single. Through experiments and simulations, the results reveal that the rotation velocity is controlled by HOP beam and self-assemble micro-structure simultaneously. Either changing the total angular momentum of driving field or changing the blade number of propeller can affect the rotation velocity. Our work may provide a simple and efficient approach for applications filed such as cell manipulation or micro-nano motors.

Reference

[1] Ashkin A, Dziedzic J M, Bjorkholm J E, et al. Observation of a single-beam gradient force optical trap for dielectric particles[J]. Optics Letters, 1986, 11(5): 288-290.

[2] Zhong M C, Wei X B, Zhou J H, et al. Trapping red blood cells in living animals using optical tweezers[J]. Nature Communications, 2013, 4: 1768.

[3] McAlinden N, Glass D G, Millington O R, et al. Accurate position tracking of optically trapped live cells [J]. Biomedical Optics Express, 2014, 5(4): 1026-1037.

[4] Lamstein J, Bezryadina A, Preece D, et al. Optical tug-of-war tweezers: shaping light for dynamic control of bacterial cells[J]. Chinese Optics Letters, 2017, 15(3): 030010.

[5] Ashkin A. Optical trapping and manipulation of neutral particles using lasers[J]. Proceedings of the National Academy of Sciences of the United States of America, 1997, 94(10): 4853-4860.

[6] Chang D E, Thompson J D, Park H, et al. Trapping and manipulation of isolated atoms using nanoscale plasmonic structures[J]. Physical Review Letters, 2009, 103(12): 123004.

[7] Li T C, Kheifets S, Medellin D, et al. Measurement of the instantaneous velocity of a Brownian particle[J]. Science, 2010, 328(5986): 1673-1675.

[8] Ashkin A, Dziedzic J M, Yamane T. Optical trapping and manipulation of single cells using infrared laser beams [J]. Nature, 1987, 330(6150): 769-771.

[9] Stevenson D J, Gunn-Moore F, Dholakia K. Light forces the pace: optical manipulation for biophotonics[J]. Journal of Biomedical Optics, 2010, 15(4): 041503.

[10] Fazal F M, Block S M. Optical tweezers study life under tension[J]. Nature Photonics, 2011, 5(6): 318-321.

[11] Huang L, Guo H L, Li J F, et al. Optical trapping of gold nanoparticles by cylindrical vector beam[J]. Optics Letters, 2012, 37(10): 1694-1696.

[12] Sifat A A, Capolino F, Potma E O. Force detection of electromagnetic chirality of tightly focused laser beams [J]. ACS Photonics, 2022, 9(8): 2660-2667.

[13] Bhebhe N, Williams P A C, Rosales-Guzmán C, et al. A vector holographic optical trap[J]. Scientific Reports, 2018, 8: 17387.

[14] Zhang L, Qiu X D, Zeng L W, et al. Multiple trapping using a focused hybrid vector beam[J]. Chinese Physics B, 2019, 28(9): 094202.

[15] Allen L, Beijersbergen M W, Spreeuw R J C, et al. Orbital angular momentum of light and the transformation of Laguerre-Gaussian laser modes[J]. Physical Review A, 1992, 45(11): 8185-8189.

[16] Bai Y H, Lü H R, Fu X, et al. Vortex beam: generation and detection of orbital angular momentum[J]. Chinese

Optics Letters, 2022, 20(1): 012601.

[17] Franke-Arnold S. Optical angular momentum and atoms [J]. Philosophical Transactions of the Royal Society A, 2017, 375(2087): 20150435.

[18] Gozali R, Nguyen T A, Bendau E, et al. Compact OAM microscope for edge enhancement of biomedical and object samples[J]. Review of Scientific Instruments, 2017, 88(9): 093701.

[19] Xin H B, Zhao N, Wang Y N, et al. Optically controlled living micromotors for the manipulation and disruption of biological targets[J]. Nano Letters, 2020, 20(10): 7177-7185.

[20] Li Y C, Liu X S, Li B J. Single-cell biomagnifier for optical nanoscopes and nanotweezers[J]. Light: Science & Applications, 2019, 8: 61.

[21] Zhu J L, Wang L, Ji J Y, et al. Real-time measurement of dynamic micro-displacement and direction using light's orbital angular momentum[J]. Applied Physics Letters, 2022, 120(25): 251104.

[22] Yan Z J, Scherer N F. Optical vortex induced rotation of silver nanowires[J]. The Journal of Physical Chemistry Letters, 2013, 4(17): 2937-2942.

[23] Donato M G, Brzobohatý O, Simpson S H, et al. Optical trapping, optical binding, and rotational dynamics of silicon nanowires in counter-propagating beams[J]. Nano Letters, 2019, 19(1): 342-352.

[24] Karpinski P. Rotation and revolution of optically trapped gold nanorods induced by the spin and orbital angular momentum of a laguerre-gaussian vortex beam[J]. Advanced Optical Materials, 2022, 10(1): 2101592.

[25] Wu X F, Ehehalt R, Razinskas G, et al. Light-driven microdrones[J]. Nature Nanotechnology, 2022, 17(5): 477-484.

[26] Milione G, Sztul H I, Nolan D A, et al. Higher-order Poincaré sphere, Stokes parameters, and the angular momentum of light[J]. Physical Review Letters, 2011, 107(5): 053601.

[27] Naidoo D, Roux F S, Dudley A, et al. Controlled generation of higher-order Poincaré sphere beams from a laser[J]. Nature Photonics, 2016, 10(5): 327-332.

[28] Zhang L, Qiu X D, Li F S, et al. Second harmonic generation with full Poincaré beams[J]. Optics Express, 2018, 26(9): 11678-11684.

[29] Yan Z. Low Reynolds number flow theory[M]. Beijing: Beijing University Press, 2002.

[30] Zhai X M, Huang W H. Calculation of light-induced force and torque on a complex microrotor by FDTD method[J]. Optics and Precision Engineering, 2008, 16(5): 778-783.